Applied Acoustics 240 (2025) 110909

Contents lists available at ScienceDirect

Applied Acoustics

journal homepage: www.elsevier.com/locate/apacoust

Low-frequency sound absorption enhancement in multi-layer honeycomb metamaterials with embedded long-curved-neck Helmholtz resonators

Ziming Song [a], Wei Chen [a,*], Shengzhe Jin [a], Hongwei Zhang [a], Feihu Shan [a], Sichao Qu [b]

[a] *Aviation Key Laboratory of Science and Technology on Additive Manufacturing, AVIC Manufacturing Technology Institute, Beijing 100024, China*
[b] *Department of Mechanical Engineering, The University of Hong Kong, 999077, Hong Kong, China*

A R T I C L E I N F O

Keywords:
Long-curved-neck resonators
Honeycomb structure
Acoustic impedance matching
Low-frequency broadband absorption
Multimodal resonance
Acoustic metamaterial

A B S T R A C T

To overcome the narrow absorption bandwidth of conventional Helmholtz resonator-based acoustic metamaterials in the low-frequency range, this study proposes a multi-layer honeycomb acoustic metamaterial with embedded long-curved-neck Helmholtz resonators (ELCN-HR). A comprehensive methodology integrating theoretical analysis, numerical simulations, and experimental testing is employed to systematically investigate the modulation of resonance frequency by neck geometric parameters and the multi-resonance mode superposition mechanism induced by hierarchical coupling. The results show that the micro-perforation diameter contributes the most in all parameters. Furthermore, the elongated ELCN-HR design substantially reduces resonance frequencies while improving acoustic wave dissipation efficiency. Additionally, the multi-layered coupling architecture excites localized resonance peaks across adjacent frequency bands, facilitating continuous spectral coupling. Optimized simulations demonstrate that the proposed metamaterial achieves a half-absorption bandwidth of 448 Hz (285–733 Hz), representing a 32% enhancement compared to conventional single-layer Helmholtz coupled structures (340 Hz). Moreover, the onset frequency for $\alpha > 0.5$ is reduced from 720 Hz to 285 Hz, significantly extending low-frequency absorption performance. Mechanistic analysis confirms that multi-scale acoustic impedance gradient matching plays a critical role in enhancing broadband energy dissipation. These findings provide a novel design paradigm for developing low-frequency broadband sound-absorbing metamaterials.

1. Introduction

In modern industrialization, noise pollution has become the third most significant environmental hazard following air and water contamination [1]. Low-to-mid frequency noise (100–1000 Hz), which is particularly prevalent in transportation infrastructure, building ventilation systems, and industrial equipment, exhibits strong penetration due to its long wavelength [2]. Conventional porous absorbers, such as fibrous materials, face inherent limitations in this frequency range, including excessive thickness (requiring dimensions equivalent to 1/4 of the wavelength) and inefficient energy dissipation. However, acoustic metamaterials, which utilize subwavelength-scale architectures, provide innovative solutions to circumvent the mass density law [3,4]. Furthermore, advances in additive manufacturing have now overcome traditional fabrication constraints, enabling more efficient noise control.

Helmholtz resonator (HR)-based metamaterials have emerged as a prominent solution due to their compact configuration and tunable low-frequency performance [5,6]. Extensive research has demonstrated that the acoustic absorption characteristics of HRs are predominantly determined by neck parameters (diameter, length, and cross-sectional geometry) and cavity morphology [7,8]. Nevertheless, their practical applicability remains significantly constrained by inherently narrowband absorption properties (typically limited to $< 1/3$ octave bandwidth), which stems from their excessively high quality (Q) factor. Current broadband strategies for HR metamaterials primarily adopt three distinct approaches: (1) Gradient structural designs that modulate neck lengths or cavity volumes to generate multiple resonance peaks [9–17]; (2) Hybrid resonance coupling that integrates multi-cavity HRs with auxiliary components such as membranes or panels to excite mixed vibrational modes [18–23]. This approach overcomes the performance limitations of conventional materials, but needs exceptionally high manufacturing

* Corresponding author.
E-mail address: werner_nju@hotmail.com (W. Chen).

https://doi.org/10.1016/j.apacoust.2025.110909
Received 29 April 2025; Received in revised form 5 June 2025; Accepted 22 June 2025

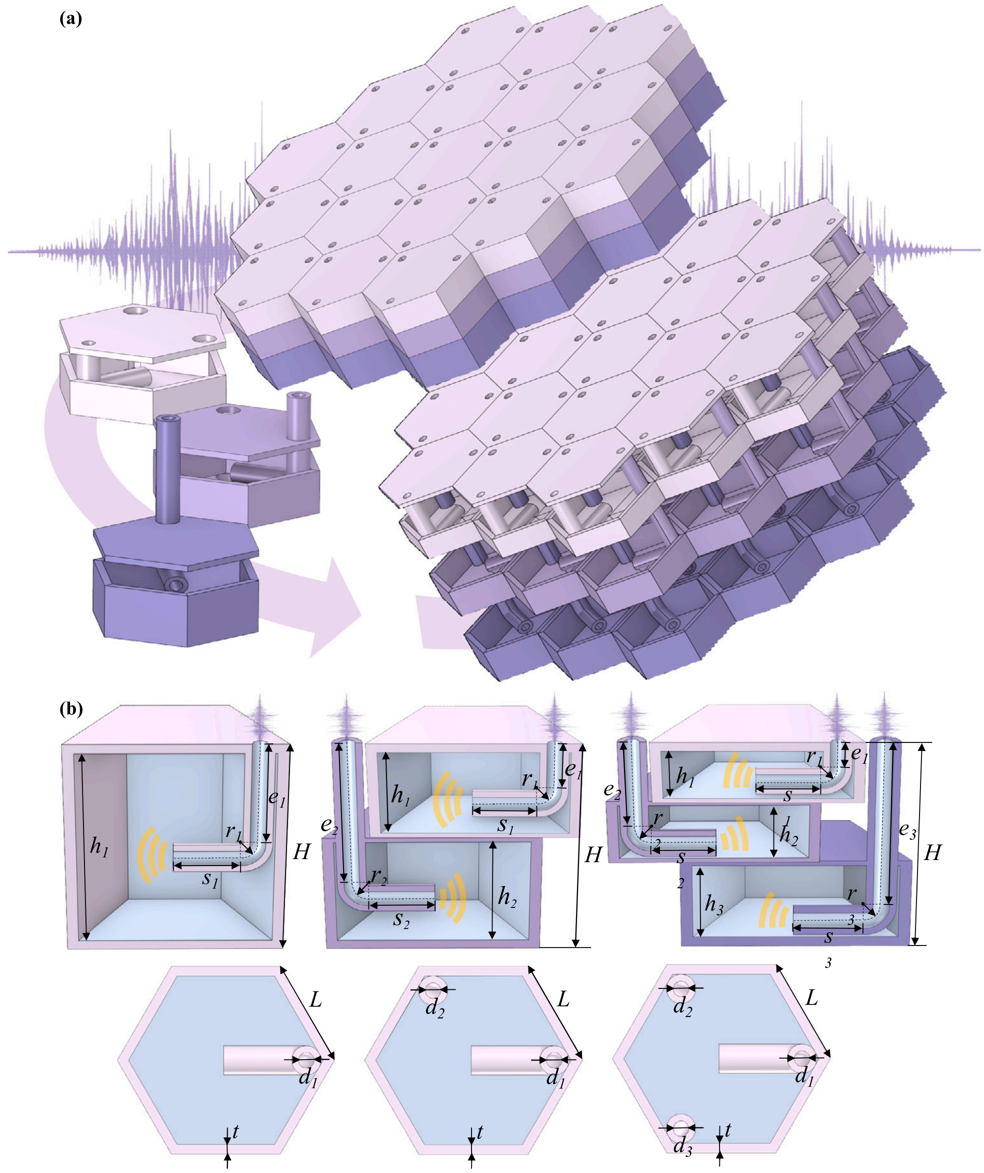

Fig. 1. Honeycomb ELCN-HR metamaterial structure: (a) overall design; (b) sound absorption mechanisms and dimensional parameters.

precision; and (3) Enhanced energy dissipation mechanisms incorporating porous media or labyrinthine channel configurations [24–34]. Recent developments have explored serrated or petaled neck designs to augment thermo-viscous losses, although these implementations encounter significant fabrication challenges due to their complex internal architectures [35–40].

These advancements highlight two persistent challenges in current HR-based metamaterials. The first one is that the inherent single-resonance narrowband absorption mechanism of conventional Helmholtz resonators fundamentally constrains effective inter-peak coupling. In addition, significant acoustic impedance mismatch occurring at resonator necks induces substantial energy reflection, particularly compromising low-frequency dissipation performance. These limitations underscore the critical need for innovative design paradigms capable of simultaneously achieving multimodal resonance excitation and graded acoustic impedance matching.

To address the demanding operational requirements in practical engineering applications, this study employs a honeycomb-based architectural framework that simultaneously offers superior out-of-plane compressive strength, enhanced shear resistance, and optimal spatial utilization [41]. Within this structural paradigm, an innovative coupled system incorporating embedded long-curved-neck Helmholtz resonators (ELCN-HR) is introduced to systematically examine the modulation effects of elongated long-curved-neck geometries and multi-layer coupling strategies on low-frequency acoustic absorption performance. The spatial coupling between the embedded long-curved-neck configuration and hexagonal cavities establishes a composite resonance system featuring graded acoustic impedance, thereby facilitating comprehensive investigation of physical mechanisms for low-frequency bandwidth enhancement. A rigorously developed finite element model demonstrates the synergistic improvement in broadband absorption through optimized acoustic impedance matching and multimodal energy dissipation in multi-layered Helmholtz cavities, while quantitatively characterizing boundary layer modulation effects arising from neck geometric curvature. Complementary experimental validation employs an acoustic testing platform to analyze key frequency-selective absorption characteristics, with microstructure characterization elucidating fundamental structure-property relationships between geometric parameters and acoustic performance metrics.

2. Structure design

The fundamental design principle of the honeycomb ELCN-HR metamaterial is to simultaneously accomplish low-frequency sound absorption through ELCN-HR and achieve broadband performance via multilayer resonance superposition. As illustrated in Fig. 1(a), each hexagonal unit cell incorporates 3 independent resonant cavities, wherein acoustic waves propagate through strategically designed curved necks before entering the k-layer (where $k = 1, 2, 3$) Helmholtz resonator chambers. Fig. 1(b) uses cutaway views to label key geometrically controlled parameters that govern its acoustic performance. These parameters include: total structure height (H), individual cavity layer height (h_k), vertical neck dimension (e_k), horizontal neck length (s_k), curvature radius (r_k), hexagonal unit cell length (L), wall thickness (t), and micro-perforation diameter (d_k). The curvature radius r_k is mathematically defined as the radius of the osculating circle to the geometric centerline of the curved neck channel, which fundamentally governs the arc length of the acoustic transmission pathway. In the schematic representation, light-blue regions demarcate the internal Helmholtz resonator cavities, while graduated color gradients differentiate the ELCN resonator structures across layers.

The honeycomb ELCN-HR architecture facilitates three-dimensional resonator alignment while preserving complete acoustic isolation between adjacent cavities, thereby significantly improving low-frequency absorption performance. This innovative configuration achieves synergistic integration of localized resonance tuning (mediated through precise neck geometry optimization) and broadband coupling effects (enabled by controlled layer interactions), ultimately establishing a dual-function mechanism for substantial bandwidth enhancement.

The sound absorption coefficient of the cavity can be derived from the following acoustic impedance equation: [42]:

$$\alpha = 1 - |R|^2 = 1 - \left|\frac{Z_s/Z_0 - 1}{Z_s/Z_0 + 1}\right|. \tag{1}$$

Here, R denotes the reflection coefficient, while $Z_0 = \rho_0 c_0$ represents the characteristic acoustic impedance of air, with ρ_0 being the ambient air density and c_0 denoting the speed of sound in air. The surface acoustic impedance Z_s of the honeycomb ELCN-HR unit cell is expressed as [42–44]:

$$Z_s = Z_n + Z_c, \tag{2}$$

where Z_s comprises two distinct components: Z_n, the surface impedance of the perforated upper panel incorporating the embedded neck structure; and Z_c, the acoustic impedance of the air contained within the hexagonal prism cavity, modified by the neck geometry. The impedance Z_n is mathematically defined as the complex ratio of the pressure differential across the aperture to the mean particle velocity, expressed as [45]:

$$Z_n = \frac{[p(z+l) - p(z)]}{v(z+l/2)}, \tag{3}$$

where $p(z) = pe^{-jk_l z}$, $v(z) = ve^{-jk_l z}$, $l = e_l + s_l + 1/4(2\pi r_l)$, substituting:

$$Z_n = \frac{(e^{-jk_l z} - e^{-jk_l})p(z)}{v(z)} = -2jZ_l \sin(\frac{k_l l}{2}). \tag{4}$$

To account for both viscous and thermal dissipation effects during sound wave propagation through the air channel of circular cross-section in the neck region, the viscous and thermal field functions, Ψ_v and Ψ_h respectively can be derived by implementing appropriate field function formulations [46]:

$$k_l{}^2 = k_0{}^2 \left(\frac{\gamma - (\gamma - 1)\Psi_h}{\Psi_v}\right), \tag{5}$$

and

$$\rho_l = \frac{\rho_0}{\Psi_v}. \tag{6}$$

Substituting Eq. (5) and Eq. (6) into Eq. (4) yields:

$$Z_n = -\frac{2j\rho_0 c_0 \sin(\frac{k_l l}{2})}{\sqrt{\gamma - (\gamma - 1)\Psi_h}}. \tag{7}$$

Due to the geometric irregularity introduced by the curved neck within the cavity, the volume velocity U of the honeycomb hexagonal prism is determined through numerical integration. The corresponding acoustic impedance Z_c of the cavity, incorporating both viscous and thermal dissipation effects, can be expressed as [45,47]:

$$Z_c = \frac{p}{v} = \frac{pS_l}{U} = -\frac{jS_l\rho_l c_l{}^2}{\omega V}, \tag{8}$$

where S_l denotes the cross-sectional area of the aperture, V represents the effective cavity volume after accounting for the neck geometry, and ρ_l is defined by Eq. (6). Incorporating the total surface area S_A of the structure with appropriate end corrections, the resultant acoustic impedance is computed as [45]:

$$Z_s = \frac{S_A}{S_l}\left(-\frac{2j\rho_0 c_0 \sin(\frac{k_l l}{2})}{\sqrt{\gamma - (\gamma - 1)\Psi_h}} - \frac{jS_l\rho_l c_l{}^2}{\omega V} + j\omega\rho_0\delta + 2\sqrt{2\omega\rho_0\eta}\right), \tag{9}$$

where η is the dynamic viscosity of air, ω represents the angular frequency, $\delta = 0.424 d_l[1 + (1 - 1.25\epsilon)]$ corresponds to the end correction for acoustic mass arising from wave radiation effects. For a regular hexagonal prism cavity, the perforation ratio ϵ is given by $\epsilon = d_l/2(l - t/\cos(\pi/6))$. An additional correction term $2\sqrt{2\omega\rho_0\eta}$ is included to account for boundary layer viscous losses due to airflow friction [42,43,45].

3. Numerical model setup

To investigate the fundamental sound absorption mechanism of the honeycomb ELCN-HR metamaterial, a three-dimensional finite element model (FEM) was developed in COMSOL Multiphysics® using the Pressure Acoustics and Thermo-viscous Acoustics modules [48–51]. The computational domain, configured according to the $k = 3$ hierarchical architecture, was discretized with the following geometric parameters: total height $H = 23$ mm, hexagonal unit cell length $L = 10$ mm, and wall thickness $t = 1$ mm (Fig. 2). All structural boundaries were modeled as acoustically rigid surfaces to simulate ideal reflection conditions.

The thermo-viscous acoustics physics interface was employed with specialized boundary layer attributes to accurately capture the thermo-viscous dissipation effects within the micro-perforated neck regions. A harmonic plane wave excitation (amplitude: 1 Pa, propagation along z-axis) was imposed on the background pressure field, while a perfectly matched layer (PML) was implemented at the top boundary to effectively absorb outgoing waves and prevent numerical reflections. Periodic boundary conditions were rigorously enforced on lateral domains to properly represent the metamaterial's hexagonal periodicity. To ensure numerical fidelity, boundary layer attributes were specifically assigned micro-perforated neck surfaces and hexagonal sidewalls. The absorption coefficient of the ELCN-HR unit cell was then quantitatively evaluated using Eq. (1).

4. Results and discussion

4.1. Parametric analysis of single-layer cavity configuration

To elucidate the acoustic performance of the honeycomb ELCN-HR unit structure, an analytical model is first developed to characterize the sound absorption behavior of a single-cavity configuration. The baseline geometric parameters of the unit cell were defined as follows: total height $H = 23$ mm, cross-sectional dimensions $L \times W = 10$ mm ×

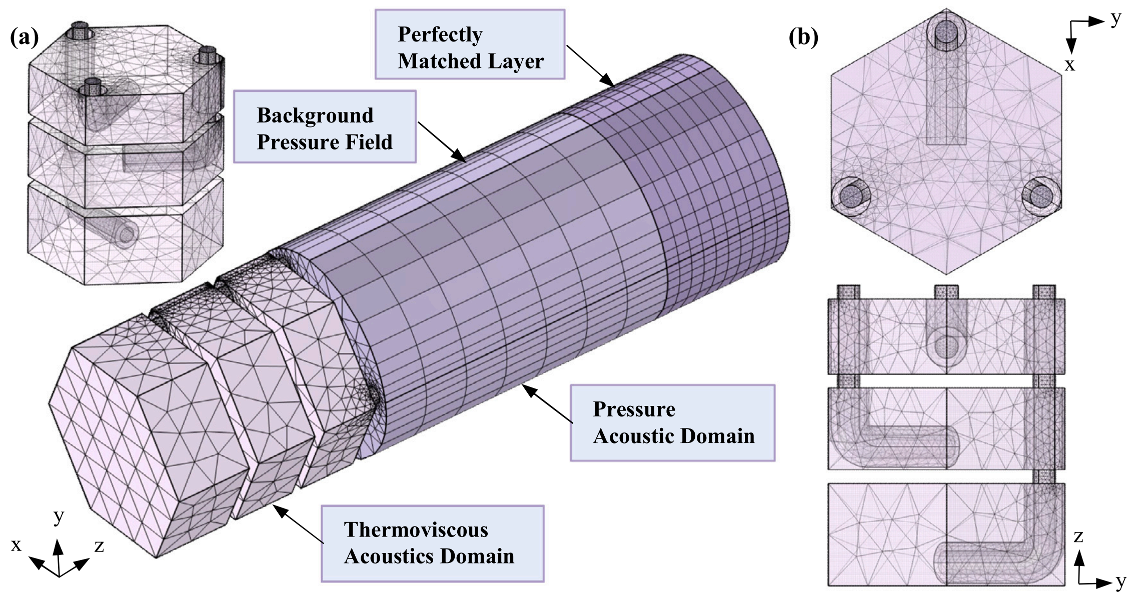

Fig. 2. Finite Element Mesh Configuration of Honeycomb ELCN-HR Unit Cell: (a) 3D Meshing Scheme; (b) 2D Cross-Sectional View of the Mesh.

Table 1
Parameter settings of the single-layer cavity.

Clusters / Parametric	A_1	A_2	A_3	B_1	B_2	B_3	C_1	C_2	C_3	D_1	D_2	D_3	E_1	E_2	E_3
Bend neck radius. r(mm)	1.5	4.5	7.5	1.5	1.5	1.5	1.5	1.5	1.5	1.5	1.5	1.5	1.5	1.5	1.5
Vertical length. e(mm)	9.5	9.5	9.5	5.0	9.5	14.0	9.5	9.5	9.5	9.5	9.5	9.5	9.5	9.5	9.5
Horizontal length. s(mm)	7.0	7.0	7.0	7.0	7.0	7.0	2.0	7.0	13.0	7.0	7.0	7.0	7.0	7.0	7.0
Cavity depth. h(mm)	21.0	21.0	21.0	21.0	21.0	21.0	21.0	21.0	21.0	21.0	13.0	17.0	21.0	21.0	21.0
Microporous diameter. d(mm)	1.7	1.7	1.7	1.7	1.7	1.7	1.7	1.7	1.7	1.7	1.7	1.7	1.4	1.7	2.0

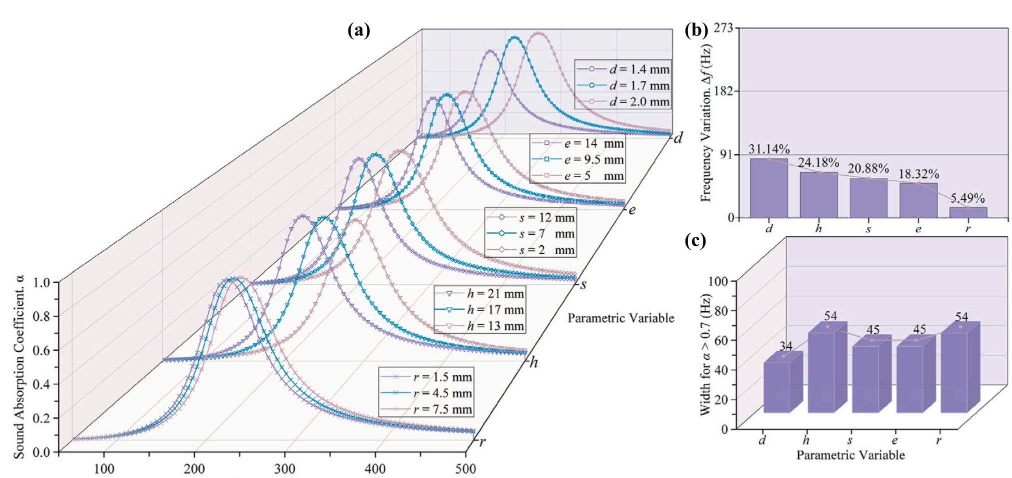

Fig. 3. Parametric Effects on Absorption Performance of Single-layer Honeycomb ELCN-HR Cavity: (a) Sound Absorption Coefficients; (b) Pareto Chart; (c) Effective Bandwidths ($\alpha > 0.7$).

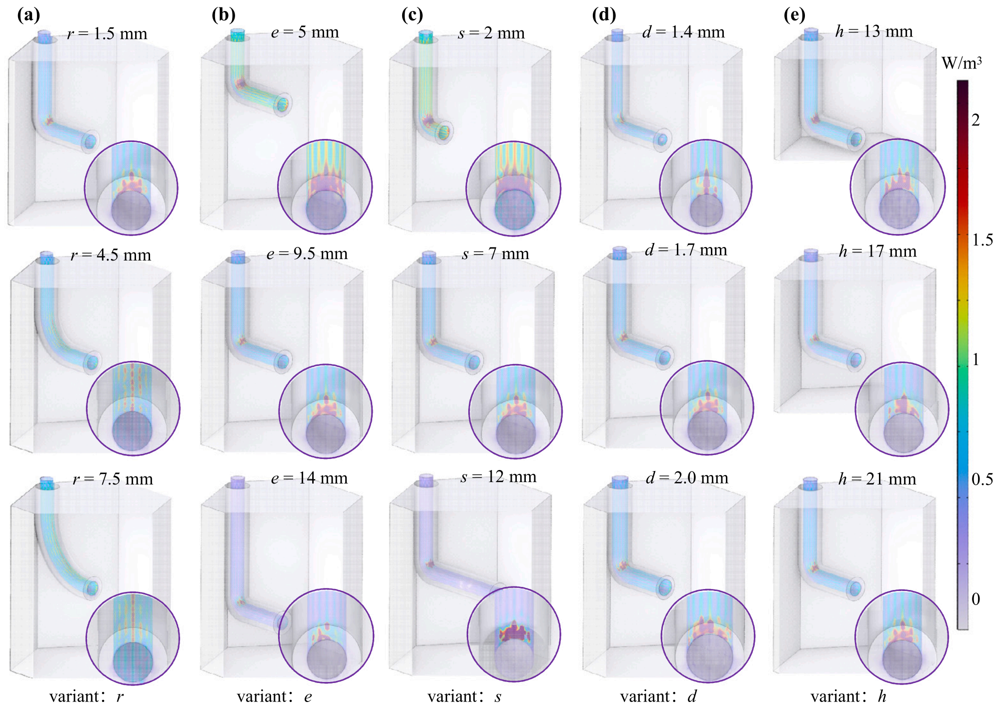

Fig. 4. Thermo-viscous Energy Dissipation in Single-layer Honeycomb ELCN-HR Cavity: (a) Bending Neck Radius r; (b) Vertical Neck Length e; (c) Horizontal Neck Length s; (d) Micro-perforation Diameter d; (e) Cavity Depth h.

10 mm, and wall thickness $t = 1$ mm. Employing a controlled-variable approach, we systematically examined the influence of key parameters of neck geometry on acoustic absorption performance, including: radius of curvature of the curved-neck centerline r, vertical neck length e, horizontal neck length s, micro-perforation diameter d, and cavity depth h. The specific parametric combinations investigated are detailed in Table 1, enabling a comprehensive evaluation of their individual and coupled effects on the sound absorption spectrum.

Numerical simulations (Fig. 3(a)) demonstrate consistent parametric trends: increasing the radius of curvature (r), vertical neck length (e), horizontal neck length (s), or cavity depth (h) induces a downward shift in resonance frequency, whereas enlarging the micro-perforation diameter (d) produces an upward frequency shift. These findings indicate that manipulating neck path complexity - either by reducing curvature radius (r) or increasing the s/e aspect ratio - along with cavity depth modulation, effectively tunes the characteristic absorption frequencies. To quantitatively assess parameter sensitivity, all variables relative to their operational ranges are normalized, resulting in normalized resonance frequency variations (Δf) across defined intervals with a cumulative frequency modulation span of 273 Hz.

Parameter contribution analysis, presented in the Pareto chart (Fig. 3(b)), reveals the micro-perforation diameter (d) exhibits the highest individual contribution rate (31.14%), substantially exceeding other parameters: cavity depth (h, 24.18%), horizontal neck length (s, 20.88%), vertical neck length (e, 18.32%), and curvature radius (r, 5.49%). This hierarchy confirms the predominant role of micro-perforation diameter in low-frequency absorption control. Of particular significance is the greater influence of horizontal neck length (s) compared to vertical length (e), suggesting enhanced acoustic impedance matching occurs in post-curvature regions during wave propagation, likely due to improved energy dissipation through optimized boundary layer interactions.

The bandwidth analysis presented in Fig. 3(c) reveals a fundamental performance trade-off inherent to single-cavity designs: while reducing the micro-perforation diameter (d) to 1.4 mm yields a lower resonance frequency of 180 Hz, this configuration suffers from a significantly constrained absorption bandwidth of merely 15 Hz. Conversely, at $d = 2.0$ mm, the system preserves a characteristic frequency of 235 Hz while achieving an 82 Hz effective bandwidth (defined at $\alpha > 0.7$ threshold). These findings provide crucial theoretical insights for multi-parameter optimization strategies, demonstrating that judicious selection of micro-perforation dimensions can effectively balance frequency targeting with bandwidth requirements in acoustic metamaterial design.

To elucidate the underlying sound energy dissipation mechanisms, Fig. 4 presents a comprehensive analysis of the internal energy distribution characteristics within the unit cell. Thermo-viscous acoustic field simulations reveal two dominant dissipation regions: (1) the inlet acoustic boundary layer, contributing approximately 12% of total energy dissipation, and (2) the neck bending zone, accounting for 81.5% of the total dissipation. As demonstrated in Fig. 4(a), a systematic reduction in the radius of curvature (r) from 7.5 mm to 1.5 mm results in a 77% enhancement of dissipation intensity within the bending zone. This finding provides direct evidence that structural asymmetry promotes vortex excitation and consequently enhances energy dissipation efficiency.

These findings establish fundamental design principles for multilayer metamaterial configurations: (1) Geometric optimization of neck architectures plays a pivotal role in maximizing viscothermal dissipation efficiency; (2) Systematic coordination between micro-perforation diameter (d) and neck dimensional parameters enables optimal trade-offs between target frequency positioning and broadband performance enhancement. Together, these principles provide a theoretical foundation for developing impedance-matched multilayer acoustic systems with tailored absorption characteristics.

4.2. Dimensional optimization of multilayer cavity configurations

To overcome the intrinsic narrowband limitations of single-cavity structures, this study presents a systematic investigation of multilayer cavity coupling mechanisms and their impact on acoustic performance enhancement. The optimization framework was implemented under fixed geometric constraints (hexagonal unit length $L = 10$ mm, wall

Table 2
Parameter settings of multilayer cavities.

Number of storeys. k \ Parametric	Storey. i	Bend neck radius r(mm)	Vertical length e(mm)	Horizontal length s(mm)	Cavity depth h(mm)	Microporous diameter d(mm)
1	1	1.5	18.0	15.5	21.0	1.8
2	1	1.5	7.0	15.5	10.0	1.8
	2	1.5	18.0	15.5	10.0	2.0
3	1	1.5	2.5	15.5	4.5	1.8
	2	1.5	9.5	15.5	7.0	1.8
	3	1.5	18.0	13.0	9.5	1.8

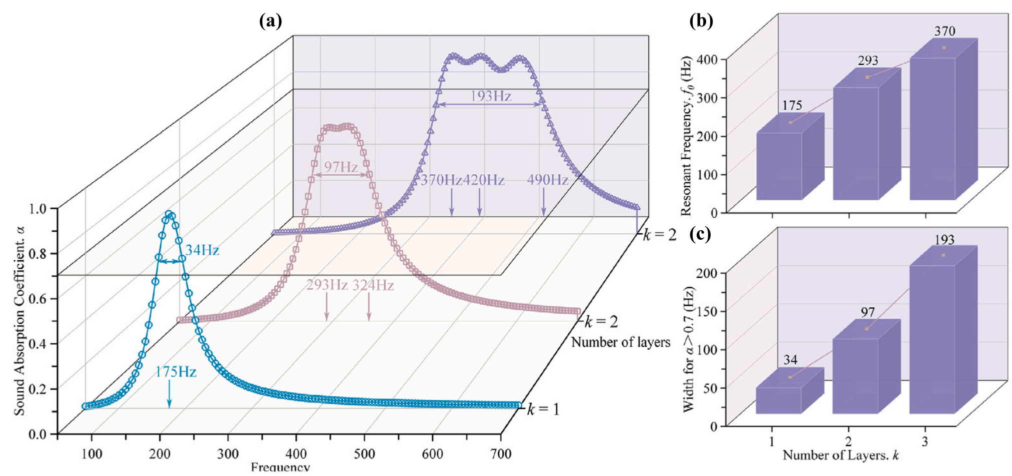

Fig. 5. Acoustic Performance Comparison of Multilayer Honeycomb ELCN-HR Cavities: (a) Sound Absorption Coefficients spectra; (b) Fundamental Resonance Frequencies f_0; (c) Effective Bandwidths ($\alpha > 0.7$).

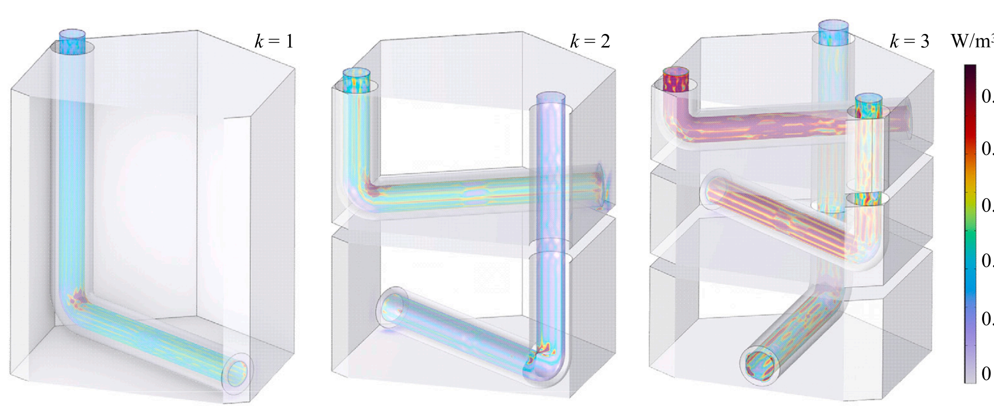

Fig. 6. Thermo-viscous Energy Dissipation in Multilayer Honeycomb ELCN-HR Unit Cells.

thickness $t = 1$ mm, total structure height $H = 23$ mm), employing the Isight multi-objective optimization platform to solve the constrained Multi-objective Optimization Problem (MOP). The optimization simultaneously targeted two key performance metrics: minimization of resonance frequency, and maximization of half-absorption bandwidth. Through this approach, optimized geometric parameters are derived, which include: Radius of curvature (r), Vertical neck length (e), Horizontal neck length (s), Micro-perforation diameter (d), Cavity depth (h). The complete set of optimized parameters is systematically presented in Table 2, with corresponding absorption coefficient frequency responses depicted in Fig. 5(a)–(c). These results demonstrate the effectiveness of the coupled multilayer design in achieving both low-frequency targeting and broadband absorption performance.

Numerical simulations reveal substantial acoustic performance enhancements through multi-layer structural design: The effective absorption bandwidth ($\alpha > 0.7$) exhibits a remarkable 467% expansion from 34 Hz (single-layer, $k = 1$) to 193 Hz (three-layer, $k = 3$) configuration, while the minimum effective absorption frequency improves by 111% (from 175 Hz to 370 Hz). These performance gains originate from carefully engineered graded interlayer dimensions that establish smooth acoustic impedance transitions, thereby significantly broadening the operational bandwidth without compromising structural compactness. The multi-layer architecture achieves an optimal compromise between low-frequency targeting and broadband performance, demonstrating clear superiority over conventional single-resonance designs.

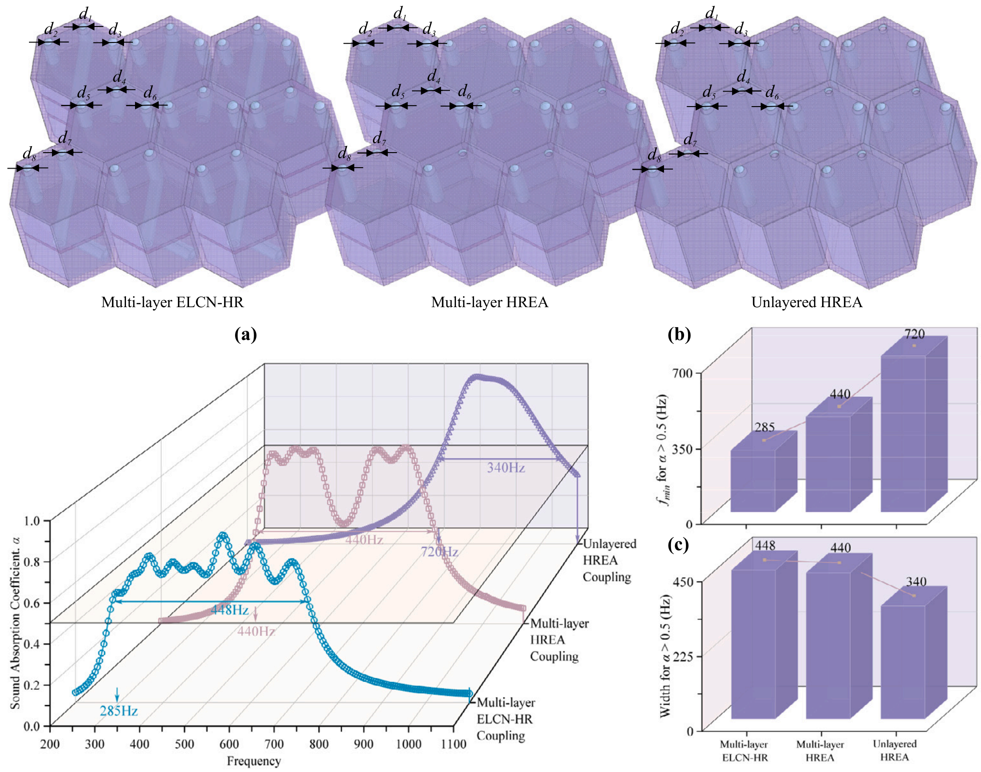

Fig. 7. Comparative Analysis of Acoustic Absorption in Coupled Multilayer Honeycomb ELCN-HR Cavities: (a) Sound Absorption Coefficients; (b) Minimum Effective Frequencies ($\alpha > 0.5$, f_{min}); (c) Effective Bandwidths ($\alpha > 0.5$).

Further investigation of the thermo-viscous acoustic fields (Fig. 6) elucidates the underlying dissipation mechanisms in the multilayer system. Simulation results indicate that maximum energy dissipation consistently occurs at the neck bending regions within each honeycomb ELCN-HR layer. Notably, increasing the horizontal neck length (s) to approach the hexagonal sidewalls enhances boundary layer effects, boosting dissipation intensity near the sidewalls by approximately 30%. Concurrently, the top-layer cavity contributes 62% of the total thermo-viscous dissipation, a phenomenon attributed to nonlinear dissipation amplification caused by pronounced velocity gradients during acoustic wave propagation. This study conclusively establishes the dual advantages of parametrically graded multilayer honeycomb ELCN-HR structures for low-to-mid frequency broadband sound absorption, providing both fundamental insights and practical design guidelines for developing next-generation acoustic metamaterials with exceptional wideband performance characteristics.

This study implemented a comprehensive multi-objective optimization framework using the Isight platform to solve the constrained Multi-objective Optimization Problem (MOP), with the objectives of minimizing fundamental resonance frequencies, and maximizing half-absorption bandwidth. Through systematic parameter space exploration, we quantitatively evaluated the acoustic performance sensitivity to five key geometric parameters: radius of curvature r, vertical neck length e, horizontal neck length s, micro-perforation diameter d, and cavity depth h. The optimization process generated a robust dataset of Pareto-optimal solutions, with representative configurations systematically documented in Table 2.

4.3. Analysis of unit structure coupling effects

To meet the critical need for effective low-to-mid frequency noise mitigation in industrial environments, this research developed an advanced multilayer honeycomb ELCN-HR coupled acoustic metamaterial through a rigorous multi-objective optimization (MOP) framework. The study focused on systematically characterizing the acoustic response within the target frequency spectrum of 200-1100 Hz to quantitatively assess performance enhancements. Three optimized unit configurations were coupled, and the absorption performance was evaluated through comparative finite element simulations.

Fig. 7 presents a systematic comparison of three distinct coupled acoustic metamaterial configurations: the proposed multilayer honeycomb ELCN-HR, multi-layer honeycomb resonators with embedded apertures (HREA), and unlayered honeycomb resonators with embedded apertures (HREA). All configurations maintain consistent hexagonal unit cell dimensions ($L = 10$ mm, $t = 1$ mm, $H = 23$ mm), identical to the single-cavity reference study, while incorporating gradient-optimized micro-perforation parameters (d_1–d_9 = 1.7, 2.1, 2.3, 1.8, 1.9, 2.1, 1.9, 2.0, 2.2 mm). The corresponding absorption coefficient frequency responses are quantitatively compared in Fig. 7(a).

The numerical simulations reveal that the optimized multilayer honeycomb ELCN-HR coupled structure demonstrates superior acoustic absorption performance in the low-to-mid frequency range (200-1100 Hz), exhibiting three distinct advantages: first, it achieves an extended half-absorption bandwidth ($\alpha > 0.5$) of 448 Hz (285-733 Hz), representing a 32% improvement over conventional unlayered HREA designs (340 Hz) while maintaining comparable performance to multi-layer HREA configurations (440 Hz); second, it significantly reduces the onset frequency for effective absorption ($\alpha > 0.5$) from 720 Hz to 285 Hz, corresponding to a remarkable 60% reduction that effectively extends the operational bandwidth to lower frequencies; and third, these performance enhancements are attributed to the optimized hierarchical coupling mechanism and improved impedance matching characteristics inherent in the novel metamaterial design. These findings collectively demonstrate the structure's potential for advanced noise control applications requiring broadband low-frequency absorption capabilities.

This significant performance enhancement can be fundamentally attributed to a precisely engineered graded impedance matching system and synergistic multi-resonance coupling effects enabled by multi-layer

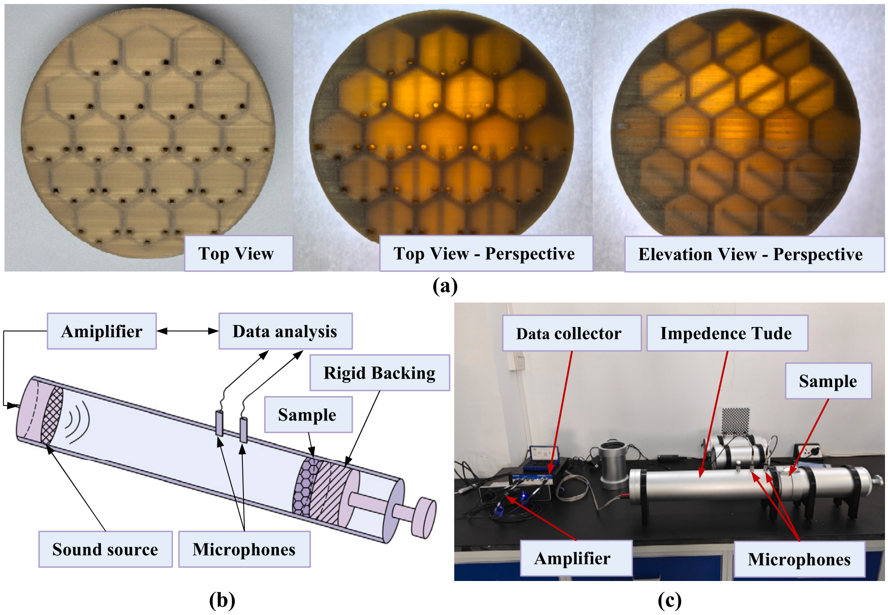

Fig. 8. Experimental Setup and Specimens: (a) Multilayer Honeycomb ELCN-HR Coupled Structure Specimen; (b) Schematic of Experimental System; (c) Impedance Tube Configuration.

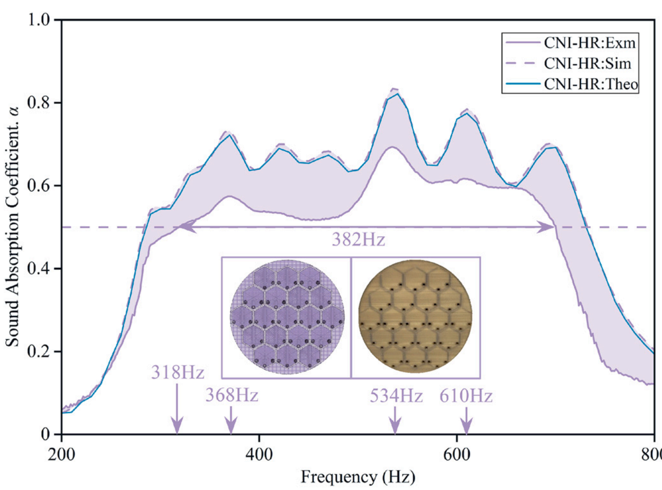

Fig. 9. Comparison of Experimental Sound Absorption Coefficients with Theoretical Calculations and Numerical Simulations.

cavity distribution. The experimental and numerical results validate the practical viability of multilayer honeycomb ELCN-HR coupled structures for industrial noise mitigation applications, particularly in the critical 200-1100 Hz frequency band.

5. Experimental and verification

To systematically evaluate the acoustic performance of the multilayer honeycomb ELCN-HR structure, comprehensive experimental investigations were conducted in conjunction with numerical simulations and theoretical analyses. As illustrated in Fig. 8(a)–(c), the sound absorption coefficients within the frequency range of 200–800 Hz were experimentally determined using a BSWA SW4201 dual-microphone impedance tube system. The testing environment was maintained under strictly controlled conditions, with an ambient temperature of 23 ± 0.5 °C and a relative humidity of 50 ± 3%. To ensure precise acoustic measurements, elastic sealing rings were employed to establish an airtight boundary between the sample and the tube walls. A linear sweep white noise signal was utilized as the excitation source, while incident and reflected acoustic waves were captured by two 1/4-inch measurement microphones positioned 20 mm apart. The sound absorption coefficients were subsequently calculated using the transfer function method.

Given the miniaturized dimensions and stringent precision requirements of the structure, additive manufacturing was utilized for specimen fabrication [52]. To meet practical engineering demands—particularly in aerospace applications involving high-vibration environments and severe impact loads—poly(ether-ether-ketone) (PEEK) was chosen as the base material due to its high elastic modulus, exceptional tensile strength, superior toughness, and impact resistance. The material properties include a density of 1300 kg/m^3, a longitudinal wave speed of 1740 m/s (at room temperature), and a printing accuracy of ±0.2 mm. To assess the acoustic performance differences between the SHR-MPP structure and conventional honeycomb configurations, specimens were fabricated in strict accordance with numerical model parameters. All structures featured an outer diameter of 98 mm, a total thickness of 23 mm (wall thickness: 1 mm), and identical micro-perforation gradients (d_1–d_9).

The specimens, comprising conventional coupled honeycomb HR and multilayer honeycomb ELCN-HR structures, were fabricated using high-temperature fused deposition modeling (FDM) with an angled monolithic printing approach. As depicted in Fig. 8(a), which presents the multilayer ELCN-HR structure with cross-sectional transparency, a 45° tilt printing strategy was employed. This orientation ensured cavity sealing integrity while eliminating the need for internal support structures by aligning all neck openings on a single side. Subsequent impedance tube testing was performed to evaluate and compare the acoustic absorption characteristics of both configurations.

The comparative results in Fig. 9 demonstrate excellent agreement between experimental measurements and theoretical/numerical predictions in characteristic peak positions (maximum deviation <2%). However, the experimental absorption peaks exhibit a 10–16% reduction relative to theoretical values, attributable to three primary factors: (1) discrepancies between the actual acoustic impedance of PEEK and theoretical assumptions; (2) limited spatial utilization (19 unit cells within the 98 mm-diameter specimen); and (3) residual standing wave effects in the impedance tube measurements. Performance analysis reveals that the multilayer honeycomb ELCN-HR coupled structure achieves a half-absorption bandwidth of 382 Hz (318–700 Hz), representing a 14%

reduction compared to theoretical predictions. This deviation primarily originates from manufacturing tolerances in the printed structures and layer-pattern effects at micro-perforation edges, which induce localized resonance frequency shifts in cavity regions.

The verification demonstrates that the multilayer coupling design effectively addresses the low-frequency limitations inherent in conventional Helmholtz resonators. Additive manufacturing proves capable of meeting the stringent precision demands for fabricating complex acoustic metamaterials, thereby providing a viable technical solution for engineering applications requiring customized sound-absorbing structures.

6. Conclusions

This study systematically investigates the acoustic modulation mechanisms and engineering potential of multilayer honeycomb ELCN-HR structures through parametric optimization, numerical simulation, and experimental validation. The key findings are:

- Parametric Sensitivity in Single-Unit Structures: Single-layer ELCN-HR structures exhibit nonlinear dependence of sound absorption performance on geometric parameters. Numerical simulations indicate that resonance frequencies can be effectively reduced by: (i) decreasing micro-perforation diameter (d), (ii) increasing horizontal neck length (s), (iii) reducing curvature radius of the neck centerline (r), or (iv) enlarging cavity depth (h). Pareto analysis quantifies d as the most influential parameter (31.14% contribution rate) for low-frequency absorption. However, the fundamental trade-off between low-frequency targeting and bandwidth expansion persists in single-cavity designs.
- Multilayer Structural Breakthrough: The hierarchical ELCN-HR architecture overcomes single-cavity limitations through coupled resonance and graded design. Maintaining constant total height ($H =$ 23 mm), increasing layers from $k = 1$ to $k = 3$ expands the effective bandwidth ($\alpha > 0.7$) from 34 Hz to 193 Hz (467% improvement). This enhancement arises from: (i) 30% increased boundary layer dissipation near sidewalls, and (ii) improved impedance matching through interlayer dimensional gradients.
- Multi-Unit Coupling Performance: The optimized multilayer structure achieves a 448 Hz half-absorption bandwidth (285-733 Hz) within 200-1100 Hz, representing a 32% improvement over conventional designs. Notably, the $\alpha > 0.5$ threshold frequency decreases from 720 Hz to 285 Hz (60% reduction), significantly extending low-frequency performance. Impedance tube experiments validate these results, showing excellent agreement among theoretical, simulated, and measured data. This advancement stems from synergistic graded impedance matching and multi-resonance coupling, enabling efficient low-frequency dissipation through precisely tuned micro-perforations and hierarchical cavity distribution.

In conclusion, this work develops a design paradigm for graded multilayer ELCN-HR structures that reconciles the low-frequency versus bandwidth trade-off through parametric optimization. The findings provide both theoretical insights and practical methodologies for engineering high-performance acoustic absorbers with significant industrial application potential.

CRediT authorship contribution statement

Ziming Song: Conceptualization, Formal analysis, Investigation, Writing – original draft. **Wei Chen:** Methodology, Writing – review & editing, Supervision, Funding acquisition. **Shengzhe Jin:** Validation, Writing – review & editing. **Hongwei Zhang:** Investigation, Software. **Feihu Shan:** Investigation, Validation. **Sichao Qu:** Writing – review & editing.

Declaration of competing interest

The authors declare that they have no known competing financial interests or personal relationships that could have appeared to influence the work reported in this paper.

Data availability

Data will be made available on request.

References

[1] World Health Organization and others. Burden of disease from environmental noise: Quantification of healthy life years lost in Europe. In: Burden of disease from environmental noise: quantification of healthy life years lost in Europe; 2011.
[2] Hollingworth G, Gilbert D. An exploratory study into the prediction of low frequency traffic noise. Appl Acoust 1982;15(2):79–96.
[3] Yang M, Sheng P. Sound absorption structures: from porous media to acoustic metamaterials. Annu Rev Mater Res 2017;47(1):83–114.
[4] Ma G, Sheng P. Acoustic metamaterials: from local resonances to broad horizons. Sci Adv 2016;2(2):e1501595.
[5] Liu Z, Zhang X, Mao Y, Zhu YY, Yang Z, Chan CT, et al. Locally resonant sonic materials. Science 2000;289(5485):1734–6.
[6] Fang N, Xi D, Xu J, Ambati M, Srituravanich W, Sun C, et al. Ultrasonic metamaterials with negative modulus. Nat Mater 2006;5(6):452–6.
[7] Bi S, Yang F, Tang S, Shen X, Zhang X, Zhu J, et al. Effects of aperture shape on absorption property of acoustic metamaterial of parallel-connection Helmholtz resonator. Materials 2023;16(4):1597.
[8] Gai X-L, Guan X-W, Cai Z-N, Li X-H, Hu W-C, Xing T, et al. Acoustic properties of honeycomb like sandwich acoustic metamaterials. Appl Acoust 2022;199:109016.
[9] Song C, Ma X, Zhao J, Zhang J, Yang F, Pan Y, et al. Broadband sound absorption and energy harvesting by a graded array of Helmholtz resonators. IEEE Trans Dielectr Electr Insul 2022;29(3):777–83.
[10] Huang J, Wang J, Ma T, Wei H, Zhang S, Wang G, et al. Composite structure with porous material and parallel resonators for broadband sound absorption at low-to-mid frequencies. Appl Acoust 2024;225:110193.
[11] Guo Z, Li Z, Zeng K, Ye J, Lu X, Lei Z, et al. Fibonacci-array inspired modular acoustic metamaterials for tunable low-frequency absorption. Adv Mater Technol 2025;10(2):2400934.
[12] Yan H, Xie S, Zhang F, Jing K, He L. Semi-self-similar fractal cellular structures with broadband sound absorption. Appl Acoust 2024;217:109864.
[13] Kang R, Shen C, Lu TJ. A three-dimensional theoretical model of free vibration for multifunctional sandwich plates with honeycomb-corrugated hybrid cores. Compos Struct 2022;298:115990.
[14] Zhang W, Xin F. Broadband low-frequency sound absorption via Helmholtz resonators with porous material lining. J Sound Vib 2024;578:118330.
[15] Bi S, Wang E, Shen X, Yang F, Zhang X, Yang X, et al. Enhancement of sound absorption performance of Helmholtz resonators by space division and chamber grouping. Appl Acoust 2023;207:109352.
[16] Kong W, Fu T. A novel butterfly double-panel metastructure filled with porous materials for broadband low-frequency sound absorption. J Build Eng 2024;97:110935.
[17] Zhang J, Chen T, Xin F, Zhu J, Ding W. New-parallel connection of the Helmholtz resonator with embedded apertures for low-frequency broadband sound absorption. Jpn J Appl Phys 2022;61(7):077001.
[18] Sun W, Wang Y, Yuan H, Guo W, Wang Y, Xue J, et al. Ultra-thin low-frequency broadband absorber based on layered coiled channel structure. Appl Acoust 2025;228:110358.
[19] Wang Y, Chen W, Liu S. Optimal ultra-broadband sound-absorption performance design for coiled up space structures with nonlinear robustness. Appl Acoust 2025;227:110236.
[20] Yang X, Shen X, Yang F, Yin Z, Yang F, Yang Q, et al. Acoustic metamaterials of modular nested Helmholtz resonators with multiple tunable absorption peaks. Appl Acoust 2023;213:109647.
[21] Chen X, Sun F, Zhang J, Chen G, Xu L, Fan L, et al. A compact acoustic metamaterial based on Helmholtz resonators with side slits for low-frequency sound absorption. Appl Phys Lett 2024;125(1).
[22] Yan S, Wu F, Zhang X, Zhang D, Wu Z. Rectangular extended neck Helmholtz resonant acoustic structure for low frequency broadband sound absorption. Phys Scr 2024;99(7):075004.
[23] Gao N, Liu J, Deng J, Chen D, Huang Q, Pan G. Design and performance of ultra-broadband composite meta-absorber in the 200hz-20khz range. J Sound Vib 2024;574:118229.
[24] Liu Y, Zeng X, Ren S, Sun W, Wang H, Lei Y. A broadband multi-resonant sound-absorbing metastructure based on impedance-matching nesting channels. Appl Acoust 2024;223:110099.
[25] Sun P, Xu S, Wang X, Gu L, Luo X, Zhao C, et al. Sound absorption of space-coiled metamaterials with soft walls. Int J Mech Sci 2024;261:108696.

[26] Cao D, Wang L, Wang J, Guo X, Li H. Design and sound absorption analysis of labyrinthine acoustic metamaterials based on fractal theory. Int J Solids Struct 2025;306:113121.
[27] Liu Z, Dong C, Tong L, Rudd C, Yi X, Liu X. Sound absorption performance of ultralight honeycomb sandwich panels filled with "network" fibers—juncus effusus. Polymers 2024;16(13):1953.
[28] Guan Y, Zhao D, Low TS. Experimental evaluation on acoustic impedance and sound absorption performances of porous foams with additives with Helmholtz number. Aerosp Sci Technol 2021;119:107120.
[29] Haris A, Lee HP. Sound transmission loss and compression properties of sandwich panels with milli-perforated honeycomb core. Fiber Polym 2022;23(11):3138–45.
[30] Nakanishi S. Broadband sound absorption by acoustic metasurface of planar array of small Helmholtz resonators. Acoust Sci Technol 2024:e24-11.
[31] Liang M, Wu H, Fu Z, Huang H, Zhang R. A compact tunable broadband acoustic metastructure with continuous gradient spiral channels. Adv Eng Mater 2023;25(10):2201577.
[32] Wu F, Xiao Y, Yu D, Zhao H, Wang Y, Wen J. Low-frequency sound absorption of hybrid absorber based on micro-perforated panel and coiled-up channels. Appl Phys Lett 2019;114(15).
[33] Gao N, Guo X, Deng J, Cheng B. Design and study of a hybrid composite structure that improves electromagnetic shielding and sound absorption simultaneously. Compos Struct 2022;280:114924.
[34] Gao N, Wang B, Lu K, Hou H. Teaching-learning-based optimization of an ultra-broadband parallel sound absorber. Appl Acoust 2021;178:107969.
[35] Song C, Huang S, Zhou Z, Zhang J, Jia B, Zhou C, et al. Perfect acoustic absorption of Helmholtz resonators via tapered necks. Appl Phys Express 2022;15(8):084006.
[36] Zhang L, Zhang W, Xin F. Broadband low-frequency sound absorption of honeycomb sandwich panels with rough embedded necks. Mech Syst Signal Process 2023;196:110311.
[37] Zhu J, Qu Y, Gao H, Meng G. Nonlinear sound absorption of Helmholtz resonators with serrated necks under high-amplitude sound wave excitation. J Sound Vib 2022;537:117197.
[38] Duan M, Yu C, He W, Xin F, Lu TJ. Perfect sound absorption of Helmholtz resonators with embedded channels in petal shape. J Appl Phys 2021;130(13).
[39] Jiang P, Jiang T, He Q. Origami-based adjustable sound-absorbing metamaterial. Smart Mater Struct 2021;30(5):057002.
[40] Yaw Z, Lai S-K, Gulzari M. Acoustic resonant metasurfaces with roughened necks for effective low-frequency sound absorption. Mech Adv Mat Struct 2024:1–13.
[41] Huang W, Zhang Y, Zhou J, Jiang F, You Y, Liu R. Stabilized and efficient multi-crushing properties via face-centered hierarchical honeycomb. Int J Mech Sci 2024;266:108918.
[42] Maa D-Y. Potential of microperforated panel absorber. J Acoust Soc Am 1998;104(5):2861–6.
[43] Ingard U. On the theory and design of acoustic resonators. J Acoust Soc Am 1953;25(6):1037–61.
[44] Wu T, Cox T, Lam Y. From a profiled diffuser to an optimized absorber. J Acoust Soc Am 2000;108(2):643–50.
[45] Huang S, Fang X, Wang X, Assouar B, Cheng Q, Li Y. Acoustic perfect absorbers via Helmholtz resonators with embedded apertures. J Acoust Soc Am 2019;145(1):254–62.
[46] Stinson MR. The propagation of plane sound waves in narrow and wide circular tubes, and generalization to uniform tubes of arbitrary cross-sectional shape. J Acoust Soc Am 1991;89(2):550–8.
[47] Huang S, Zhou Z, Li D, Liu T, Wang X, Zhu J, et al. Compact broadband acoustic sink with coherently coupled weak resonances. Sci Bull 2020;65(5):373–9.
[48] Mukae S, Okuzono T, Tamaru K, Sakagami K. Modeling microperforated panels and permeable membranes for a room acoustic solver with plane-wave enriched fem. Appl Acoust 2022;185:108383.
[49] Zhao H, Zheng Q, Wang Y, Cao J, Wang C, Wen J. Acoustic absorption of a metamaterial panel: mechanism, boundary effect and experimental demonstration. Appl Acoust 2021;184:108369.
[50] Uenishi K, Okuzono T, Sakagami K. Finite element analysis of absorption characteristics of permeable membrane absorbers array. Acoust Sci Technol 2017;38(6):322–5.
[51] Okuzono T, Shimizu N, Sakagami K. Predicting absorption characteristics of single-leaf permeable membrane absorbers using finite element method in a time domain. Appl Acoust 2019;151:172–82.
[52] Carbajo J, Molina-Jordá JM, Maiorano L, Fang NX. Sound absorption of macro-perforated additively manufactured media. Appl Acoust 2021;182:108204.